Astron. Astrophys. 363, 84–92 (2000)

ASTRONOMY AND ASTROPHYSICS

Parsec-scale structures of radio galaxies in the 2-Jy sample

T. Venturi[1], **R. Morganti**[2], **T. Tzioumis**[3], **and J. Reynolds**[3]

[1] Istituto di Radioastronomia del CNR, Via Gobetti 101, 40129 Bologna, Italy
[2] Netherlands Foundation for Radio Astronomy, Postbus 2, AA 7990 Dwingeloo, The Netherlands
[3] ATNF-CSIRO, P.O. Box 76, Epping, NSW 2121, Australia

Received 4 August 2000 / Accepted 25 August 2000

Abstract. In this paper we present the results of VLBI observations of six radio galaxies belonging to the 2-Jy sample. The selected objects are 3C17, PKS 0620−52, PKS 0625−35, PKS 1318−43, PKS 1333−33 and 3C317. The first is a high power radio galaxy and the remainder are all low power objects. Our observations were carried out with a set of different arrays and frequencies, and cover a range of resolutions from a few mas to a few tens of mas.

Parsec-scale images are presented and discussed in the light of unification for radio loud galaxies. Estimates for the intrinsic plasma speeds in these objects in the proximity of the parsec-scale core and their orientation to the line of sight are in agreement with the predictions from unified models and with their optical and X-ray properties.

We will use H_o = 50 km s^{-1}Mpc^{-1}, q_o = 0 and $S \propto \nu^{-\alpha}$ throughout the paper.

Key words: galaxies: general – galaxies: quasars: general – galaxies: structure – radio continuum: galaxies

1. Introduction

The study of the nuclear regions in radio galaxies with Very Long Baseline Interferometry (VLBI) has proved to be a very important tool for the understanding of the properties of the central engine in low and high power radio galaxies. Furthermore it has provided a major contribution in testing the unified schemes which attribute the main differences between the various classes of AGNs to relativistic beaming and orientation effects.

VLBI observations of complete samples of radio galaxies, together with detailed observations on individual objects (see for example Feretti et al. 1993; Venturi et al. 1993 and 1995; Giovannini et al. 1994, 1998, 1999; Lara et al. 1997 and 1999; Jones & Wehrle 1997; Krichbaum et al. 1998; Taylor 1996), show that lobe-dominated, edge-darkened low power FRI radio galaxies and the lobe-dominated, edge-brightened high power FRIIs (Fanaroff & Riley 1974) are almost indistinguishable on the parsec scale.

Both classes of radio galaxies are typically characterised by one-sided parsec-scale morphology. A few cases of symmetric two-sided morphologies are found both among FRIs, i.e. Hydra A (Taylor 1996) and 3C338 (Giovannini et al. 1998), and among FRIIs, for example 3C452 (Venturi et al. 2000, Giovannini et al., in preparation). From these studies, relativistic bulk motion of the radio emitting plasma in the radio jets, with Lorentz factors ranging from a few units up to 10 were derived.

For both classes of objects it is estimated that the radio emission is oriented at intermediate to large angles to the line of sight. This is in agreement with predictions from the standard unified models where FRII radio galaxies represent the misaligned population of flat spectrum quasars (Barthel 1989), while FRIs are the misaligned population of BL-Lac objects (Urry & Padovani 1995). For the latter unification, there remain some issues to be clarified. For example, on the basis of statistical arguments and optical data, Chiaberge et al. (1999, 2000) and Capetti & Celotti (1999) concluded that the Lorentz factors needed for FRIs and BL-Lacs, in order to account for the different orientation dependent properties, are in the range $\gamma \sim$ 3–7. These values are lower than derived by independent arguments, such as the modelling of the spectral energy distribution in BL-Lacs (Ghisellini et al. 1998).

Chiaberge et al. (2000) proposed that a two-phase jet in FRIs could account for the apparent discrepancy in the standard unification model. Furthermore they underlined the importance of multifrequency studies of the nuclear regions of radio galaxies and their parent aligned population, in order to overcome the remaining discrepancies between theoretical predictions and observations, and to probe the inner parsec-scale regions in AGN.

In addition, radiative inefficient accretion models, such as the Advection Dominated Accretion Flow (ADAF), have been recently suggested to explain the spectral properties of some radio galaxies. In particular, they have been applied to galaxies with high hard X-ray excess and moderate radio luminosity (see e.g. Di Matteo et al. 1999) but no sign of AGN activity from the optical lines. Milliarcsec resolution radio observations provide parsec-scale imaging of the innermost regions in radio galaxies, and allow derivation of the radio spectrum of the nuclear component, both crucial pieces of information to test and constrain the ADAF accretion process.

Given the importance of multi-wavelength information, as emphasized above, we have started a program to provide VLBI information for some of the radio sources in the 2-Jy sample.

Send offprint requests to: T. Venturi (tventuri@ira.bo.cnr.it)

Table 1. The sources in the VLBI sample

Source	Other Name	RA. (1950)	Dec. (1950)	z	S_c (5 GHz) Jy	logP_c (5 GHz) W Hz^{-1}	logP_t (408 MHz) WHz^{-1}	Type
0035−02	3C 17	00 35 47.17	−02 24 09.3	0.220	0.662	26.21	27.55[1]	FRI/II
PKS 0620−52		06 20 36.85	−52 40 00.9	0.051	0.260	24.49	25.90[1]	FRI
PKS 0625−35	OH 342	06 25 20.22	−35 27 22.0	0.055	0.600	24.91	26.02[1]	FRI
PKS 1318−43	NGC 5090	13 18 17.40	−43 26 33.4	0.011	0.580	23.49	24.32*	FRI
PKS 1333−33	IC 4296	13 33 47.16	−33 42 39.8	0.013	0.297	23.35	25.41[2]	FRI
1514+07	3C 317	15 14 16.99	+07 12 17.1	0.035	0.391	24.34	26.12[1]	C/H

References: [1] Large et al., 1981; [2] Wright & Otrupcek 1990.
* No 408 MHz power is available in the literature. See Sect. 5 in text.

For the sources in this sample a wealth of radio, optical, X-ray data are already available. In this paper we present VLBI radio observations of the nuclear region in six radio galaxies selected from this sample not yet imaged at parsec-scale resolution, and discuss them in the light of their large scale radio properties, optical and X–ray features. In Sect. 2 we illustrate the selection criteria and give an overview of the selected sources; the observations and data reduction are described in Sect. 3; individual sources are discussed in Sect. 4. Discussion and conclusions are given in Sect. 5.

2. Selected radio galaxies from the 2-Jy sample

Radio sources belonging to the 2-Jy catalogue of radio sources (Wall & Peacock 1985) are potentially a very useful tool for the understanding of the nuclear properties of radio galaxies. The 2-Jy sample is well studied in a wide range of wavelengths, from radio (Morganti et al. 1993, 1999 and references therein), to optical spectroscopy (Tadhunter et al. 1993, 1998 and references therein), up to X–ray energies (Siebert et al. 1996, Trussoni et al. 1999, Padovani et al. 1999). Recently, 23 galaxies in the sample have also been searched for HI absorption (Morganti et al. 2000). This allows comparative studies, which are crucial to understand the physics of the inner parsec-scale region of AGN, and to test unified models and evolutionary scenarios.

The 2-Jy sample includes radio sources with flux density $S_{2.7\,GHz} \geq 2$ Jy, redshift z < 0.7 and declination $\delta \leq +10°$. Given the frequency of observation, the sample is biased towards beamed radio sources.

Among the 2-Jy sample we have selected all sources with S_{core} (5 GHz) ≥ 200 mJy not yet imaged at VLBI resolution. The core flux density limit was chosen so as to be able to image the southernmost radio galaxies with the sensitivity of the southern Long Baseline Array (LBA) at the time the original proposals were made. In this paper we present the results of parsec-scale observations for six radio galaxies from the selected sample. The list of objects is given in Table 1, where the most relevant parameters, i.e. redshift z, core power logP_c at 5 GHz (data taken from Morganti et al. 1993) and total power logP_t at 408 MHz are also reported.

Among them we have four classical FRIs, one core-halo source and one intermediate type FRI/FRII. The power range of 3C17 is typical of FRIIs, however its arcsecond scale morphology is more similar to the transition objects between FRIs and FRIIs than to the typical classical doubles (Morganti et al. 1993; Morganti et al. 1999). It is the most distant object among the sources in the present sample. The total power for the five remaining galaxies is that of the most powerful FRIs, and their large scale radio emission is typical of FRI except for 3C317, which is classified as core-halo.

PKS 0625−35, PKS 1333−33 and 3C317 are all located in Abell clusters, respectively A3392, A3565 and A2052; PKS 1318−43 is located in a low density environment and it is interacting with the peculiar companion galaxy NGC5091. Very little information is available on the galaxy cluster surrounding PKS 0620−52; finally the large scale environment of 3C17 is unknown.

3. Observations and data reduction

Our VLBI observations were carried out at various frequencies, with different array configurations and recording modes. The logs of the observations, together with the most relevant information, are given in Table 2. The bandwidth of the MK2 observations is 2 MHz; the S2 observations were carried out with a single 16 MHz band; the MK3 observations were carried out in mode E, with 7 IFs and a total bandwidth of 14 MHz.

The initial part of the data reduction (a-priori amplitude calibration and phase correction) was carried out differently for the various experiments, given the different formats of the correlator output; self-calibration and imaging were performed by means of the NRAO AIPS package for all sources. Data correlated with the 5 station Block 0 MK2 correlator in Bologna were written into merge format and read into the Caltech package (Pearson 1991) for the a-priori calibration; both the S2 data correlated in Epping and the MK3 data correlated in Bonn were read into AIPS, where fringe-fitting, self-calibration and imaging were carried out.

Because of the different array configurations and sensitivities, the resolution and quality of our final images vary from case to case. The flux density scale is accurate within a few percent for 3C17 (MK2 - VLBA observations) and for 3C317 (EVN+Merlin MK3 observations), while for all sources observed with LBA the uncertainties are of the order of 10–15%.

Table 2. Logs of the VLBI observations

Source	Date	Array	ν GHz	Min.- Max. Baseline Mλ	Mode	Duration hr	Correlator
3C17	02/10/94	VLBA[1]	4.99	7.3–145	MK2	8	Bologna
PKS 0620−52	22/06/96	LBA[2]	2.29	0.7–10.3	S2	8	Epping
PKS 0625−35	23/02/94	LBA[3]	2.30	0.7–10.7	MK2	8	Bologna
PKS 1318−43	24/02/94	LBA[3]	2.30	0.4–10.6	MK2	8	Bologna
PKS 1333−33	23/06/96	LBA[2]	2.29	0.8–10.7	S2	8	Epping
3C317	14/02/95	EVN+MERLIN[4]	1.66	0.1–36.5	MK3-E	10	Bonn
3C317	13/05/96	EVN+MERLIN[5]	4.99	0.03–12.5	MK3-E	10	Bonn

[1] Seven VLBA antennas: SC, HN, NL, PT, OV, BR, MK
[2] Five LBA antennas: Parkes, Mopra, Compact Array (single antenna), Tidbinbilla, Hobart
[3] Five LBA antennas: Parkes, Mopra, Compact Array (single antenna), DSS45, Hobart
[4] Five EVN antennas: Cambridge, Jodrell Bank, Noto, Medicina, Onsala
[5] Five EVN antennas: Effesberg, Jodrell Bank, Noto, Medicina, Onsala

Table 3. Details on the images

Source	ν GHz	Restoring FWHM mas	rms mJy b^{-1}	S$_{core}(VLBI)$ mJy	S$_{tot}(VLBI)$ mJy	S$_{PTI}$ (2.3GHz) mJy	Figure #
3C17	4.99	3.6×1.4	0.38	316	465	411	1
PKS 0620−52	2.29	33.5×11.4	0.95	80	80	123	2
PKS 0625−35	2.29	33.1×13.7	0.37	507	554	536	3
PKS 1318−43	2.29	30.0×15.0	0.86	353	407	411	4
PKS 1333−33	2.29	72.4×19.9	0.67	128	128	188	5
3C317	1.66	233.0×97.4	1.31	341	349	310	6
3C317	4.99	57.9×43.9	0.28	355	359	-	7
3C317	4.99	5.0×2.0	0.33	296	360	-	9

4. Comments on individual sources

We report the images of the six radio galaxies in Figs. 1 through 9, and describe them in detail in the following subsections. In agreement with the results found in the literature on the parsec-scale morphologies of radio galaxies, our objects are either dominated by a nuclear component with asymmetric jet emission, or show only marginal extension. In Table 3 we give the observational parameters of the images, i.e. the total VLBI flux density and the flux density in the most compact component, assumed to be the core. For the unresolved sources these two values are coincident. For comparison we report also the 2.3 GHz core flux density measured with the Parkes-Tidbinbilla real-time interferometer (PTI, Morganti et al. 1997), while the flux density of the arcsecond scale nucleus at 5 GHz (Morganti et al. 1993) is given in Table 1.

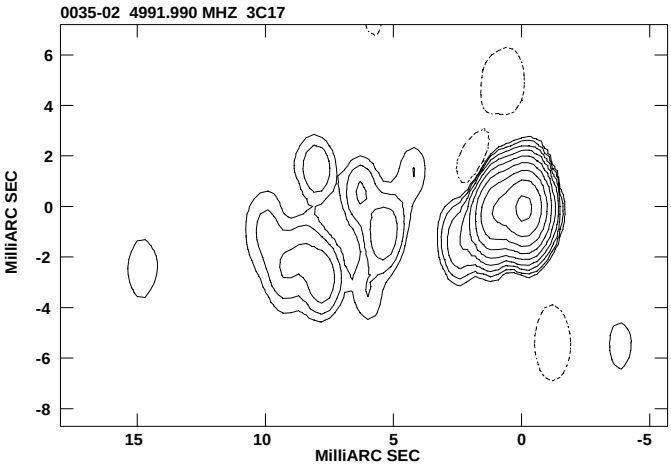

Fig. 1. 5 GHz image of 3C17. Peak is 275 mJy/beam. Contours are 0.9 mJy/beam × (-1, 1, 2, 4, 8, 16, 32, 64, 128, 256). Beam FWHM: 2.0 × 1.0 (mas) at 0°. For this source 1 mas ∼ 4 pc.

4.1. 0035−02 (3C17)

This is the most powerful and most distant object in our sample. It is classified as a broad line radio galaxy (Tadhunter et al. 1993) and it is also characterised by optical polarisation (Tadhunter et al. 1997). High resolution 5 GHz VLA observations (Morganti et al. 1999) show that the source is very asymmetric on the arcsecond scale both in shape and brightness. The south-east arcsecond scale jet is aligned in position angle (p.a.) $\sim +100°$, and it is characterised by high brighness knots. It sharply bends by $\sim +200°$ at ~ 10 arcsec from the core. No jet is visible on the north-western side, but only a diffuse lobe, with a ring-like structure, at ~ 5 arcsec in projected distance form the core. ROSAT X–ray emission was detected by Siebert et al. (1996).

Our parsec scale image, given in Fig. 1, shows a one-sided morphology oriented in east-west at $\sim +100°$, roughly in agree-

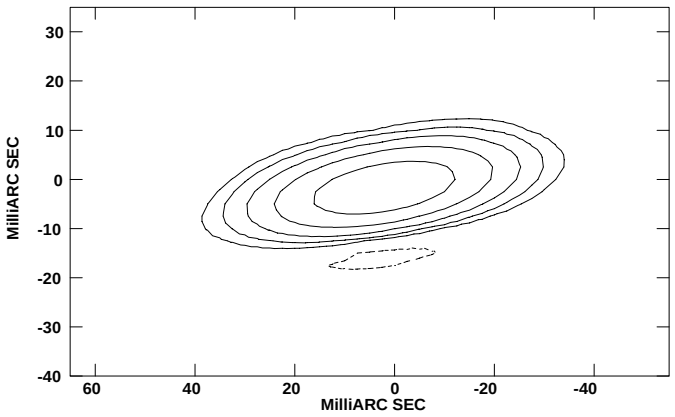

Fig. 2. 2.29 GHz image of PKS 0620−52. Peak is 80 mJy/beam. Contours: 3.0 mJy/beam × (-1, 1, 2, 4, 8, 16, 32, 64, 128, 256). Beam FWHM: 33.5 × 11.4 (mas) at -84°. For this source 1 mas $\sim$ 1.4 pc.

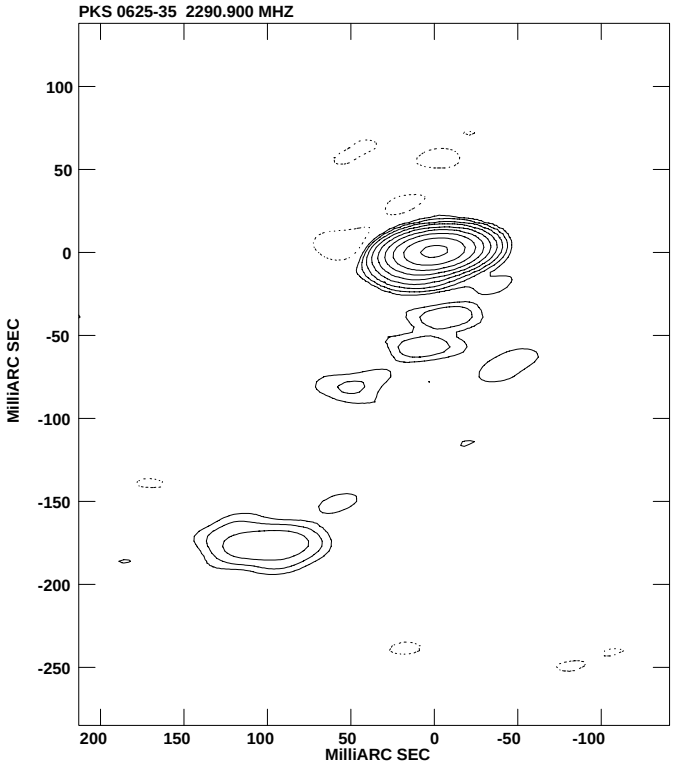

Fig. 3. 2.29 GHz image of PKS 0625−35. Peak is 490 mJy/beam. Contours: 1.2 mJy/beam × (-1, 1, 2, 4, 8, 16, 32, 64, 128, 256). Beam FWHM: 33.1 × 13.7 (mas) at -84.3°. For this source 1 mas $\sim$ 1.5 pc.

ment with the initial orientation of the south-east arcsecond scale jet. Using the AIPS task JMFIT on this image, we performed a multi-component gaussian fit of the inner 5 mas. The source can be described with an unresolved component, the westernmost one, which we identify with the core of the radio emission on the basis of its compactness, and two more compact components. The component parameters derived from our fit are given in Table 4, where we report the flux S, size and position angle (p.a.) of each component, the distance and position angle (P.A.) from the core for the secondary components along the parsec-scale inner jet, listed in order of increasing distance from the core.

4.2. PKS 0620−52

This radio source is associated with the brightest member of a galaxy cluster, and its arcsecond scale morphology is typical of this large scale environment, since it exhibits a wide-angle tail morphology with two asymmetric tails (Morganti et al. 1993). Very little optical information is available for this source and its surroundings. BeppoSAX X–ray observations were not conclusive with respect to the existence of a non-thermal X–ray component of nuclear origin (Trussoni et al. 1999).

PKS 0620−52 is the weakest source in our VLBI sample and it is unresolved by the present 2.29 GHZ observations. The image is shown in Fig. 2. Assuming that flux density variations in this source are negligible, comparison with the 2.3 GHz PTI flux (see Table 3), suggests that extended flux, not imaged by our observations, must be present on the sub-arcsecond scale. The spectrum of the source in the range 2.3–5 GHz is typical of gigahertz peaked sources (GPS).

4.3. PKS 0625−35 (OH 342)

The arcsecond scale emission for this radio galaxy is dominated by a bright core, with a one-sided jet in p.a. $\sim +160^\circ$, embedded in a low brightness halo (Simpson 1994), which extends out to $\sim 4'$ in the low resolution image of Ekers et al. (1989). X–ray BeppoSAX observations (Trussoni et al. 1999) are in agreement with the presence of a non-thermal hard X–ray component, likely to be of nuclear origin. The X–ray emission from the central region appears unabsorbed. These observational properties could be interpreted either as the source being oriented at a small angle to the line of sight or that it is not heavily affected by obscuration from a circumnuclear torus.

Our VLBI image, shown in Fig. 3, is in agreement with its arcsecond scale structure. It is dominated by a strong central component, which contains $\sim 90\%$ of the total VLBI flux density, with a faint jet aligned in p.a. $\sim 150^\circ$. The flux density given in Table 3 is consistent with the PTI 2.3 GHz value if we account for the large uncertainties in the flux density scale for the LBA observations (see Sect. 3).

From Fig. 3 and from another image restored with a slightly super-resolved restoring beam in p.a. 0° (not shown here) it is clear that the dominant component is resolved and shows an extension in p.a. $\sim +130^\circ$. With the AIPS task JMFIT we resolved it into two components. Details on the fitting parameters are given in Table 4. The southernmost jet component visible in Fig. 3 is very diffuse. It is located at $\sim +200$ mas, and has a total flux density of ~ 28 mJy.

4.4. PKS 1318−43 (NGC 5090)

This source is a typical FRI radio galaxy (Morganti et al. 1993; Lloyd et al. 1996), with symmetric arcsecond scale jets and a total extension of ~ 17 arcmin. The most prominent feature of

Table 4. Results from the gaussian fit

Source	ν GHz	Component	Flux mJy	Size mas	p.a.	Dist. from core mas	P.A.
3C17	4.99	Core	316	< 0.54	-		
		1st	113	< 0.63	-	1.19	95°
		2nd	8	< 0.74	-	2.96	110°
PKS 0625−35	2.29	Core	507	4.1× 1.0	161.3°		
		1st	20	< 8.3	-	19.2	130°
PKS 1318−43	2.29	Core	353	< 4.6	-		
		1st	53	< 10.5	-	18.8	50°

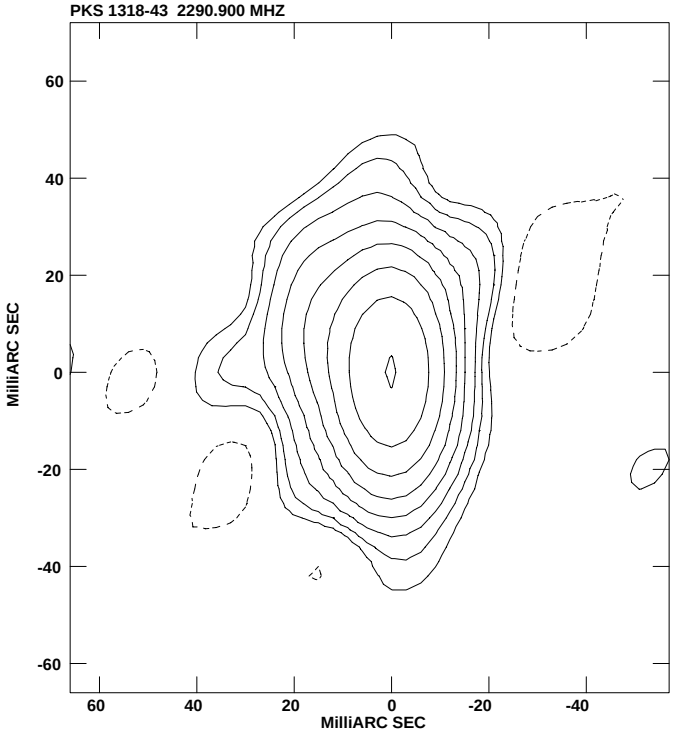

Fig. 4. 2.29 GHz image of PKS 1318−43. Peak is 345 mJy/beam. Contours: 2.6 mJy/beam × (-1, 1, 2, 4, 8, 16, 32, 64, 128, 256). Beam FWHM: 30×15 (mas) at 0°. For this source 1 mas ∼ 0.3 pc.

the arcsecond scale jets is their strong S-bend shape, from the region closest to the core out to the end of the jets (Lloyd et al. 1996). One possible explanation for this interesting structure comes from the local environment of the optical counterpart, which is believed to be interacting with the nearby spiral galaxy NGC 05091 (Smith & Bicknell 1986). HI absorption has been detected (using the VLA) against the core of this galaxy. The HI profile appears double peaked and the HI velocity derived is very close to the systemic velocity of the galaxy (v = 3421 km s^{-1}).

The parsec-scale morphology of PKS 1318−43 is shown in Fig. 4. This image was obtained including only the baselines in the range 0–8.5 Mλ, given the very noisy data on the longest baselines (due to the lower sensitivity of the array) and it was convolved with a restoring beam oriented in p.a. 0°, so as to better show its extension. From Fig. 4 it is clear that the source is resolved, and we fitted it with two componens, i.e. a dominant compact one, which we assume to be the radio core, and a secondary peak at ∼ 18.8 mas, in p.a. ∼ +50°, aligned with the northern arcsecond-scale jet. Details on the fit are reported in Table 4.

The total flux density on the VLBI scale (see Table 3) is in good agreement with the 2.3 GHz PTI data. Our value, coupled with the radio data for the arcsecond radio nucleus of PKS 1318−43 collected from the literature (Table 3 and Lloyd et al. 1996), suggest that the radio nucleus is self-absorbed at least up to $\nu = 8.6$ GHz.

4.5. PKS 1333−33 (IC 4296)

PKS 1333−33 is a very large radio galaxy (Killeen et al. 1986), with radio power typical of transition objects between FRI and FRII sources (see Table 1). Its radio morphology reflects the radio power, and it is also intermediate between these two classes. The source is characterised by an arcsecond self-absorbed nucleus, which peaks at $\nu \sim 15$ GHz, and by two symmetric knotty jets which culminate in two "warm" spots at a distance of $\sim 12''$ from the core, i.e. ~ 250 kpc. The associated optical counterpart is a nearby elliptical galaxy, with a featureless optical spectrum. X–ray observations carried out with ASCA and BeppoSAX (Fiore et al. in preparation), revealed the existence of a hard X–ray excess over the thermal stellar component, most likely of nuclear origin, which led them to propose that a low efficiency accretion flow is hosted in the nuclear region of the galaxy.

PKS1333−33 is almost unresolved at the resolution and sensitivity of the present 2.29 GHz observations. As for PKS 1318−43, due to sensitivity limits, the very noisy data points on the longest baselines forced us to taper the u-v coverage in order to get a reliable image, thus degrading the FWHM. Deconvolution of the image presented in Fig. 5, carried out with the program JMFIT in the AIPS package, shows that it can be fitted with a gaussian component of the size of ∼ FWHM/4. The flux density value given in Table 3 is in good agreement with the arcsecond core spectrum given in Killeen et al. (1986) and with the PTI 2.3 GHz data (Morganti et al. 1997), allowing for the different resolution of our VLBI image. However, comparison with the PTI data confirms our estimate that the uncertainties on the absolute flux density scale may be of the order of ∼ 10–15%.

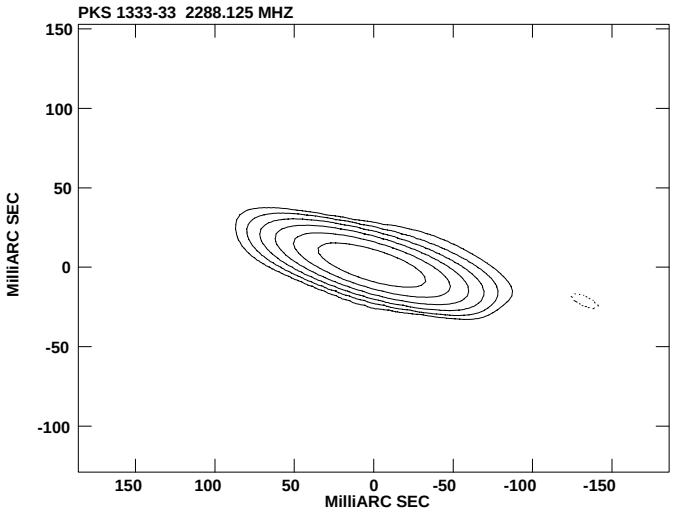

Fig. 5. 2.29 GHz image of PKS 1333−33. Peak is 119 mJy/beam. Contours: 2.0 mJy/beam × (-1, 1, 2, 4, 8, 16, 32, 64, 128, 256). Beam FWHM: 72.4 × 19.9 (mas) at 72.1°. For this source 1 mas ∼ 0.4 pc.

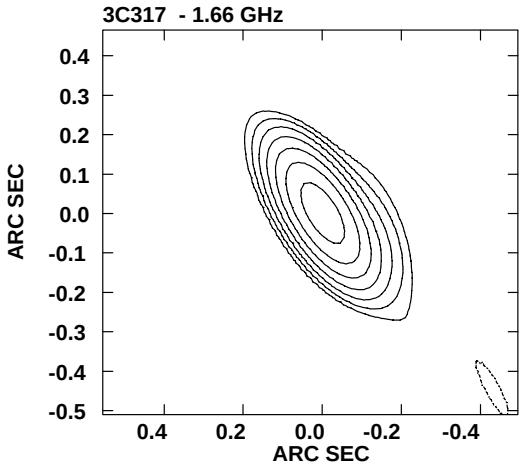

Fig. 6. 1.66 GHz MERLIN-only image 0f 3C317. Peak: 341 mJy/beam. Contours: 3.6 mJy/beam × (-1, 1, 2, 4, 8, 16, 32, 64, 128, 256). Beam FWHM: 233.0 × 97.4 (mas) at 31.2°. Linear scale: 1 mas ∼ 1 pc.

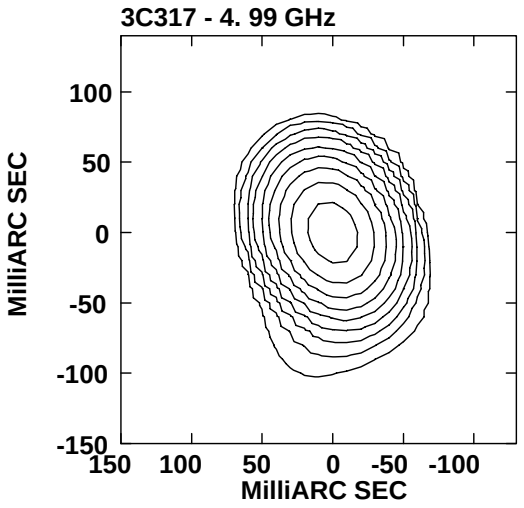

Fig. 7. 4.99 GHz MERLIN-only image 0f 3C317. Peak: 353 mJy/beam. Contours: 0.9 mJy/beam × (-1, 1, 2, 4, 8, 16, 32, 64, 128, 256). Beam FWHM: 57.9 × 43.9 (mas) at 24.2°. Linear scale: 1 mas ∼ 1 pc.

4.6. 3C317

3C317 is one of the best studied radio sources in our VLBI sample. It is associated with the cD galaxy UGC 9799, at the centre of the cooling flow cluster of galaxies A2052. Its radio power is typical of FRI radio galaxies. The source was imaged with the VLA in a wide range of frequencies and studied in detail by Zhao et al. (1993). According to its morphology it can be classified as core-halo, in that it is characterised by a compact region surrounded by a steep spectrum low brightness radio halo. It has an angular extent $\sim 1.5'$ ($\sim$ 100 kpc) and it is all embedded within the optical galaxy. The inner arcsecond scale region of 3C317 is characterised by a counter-clockwise bent morphology, in a spiral-like shape. The source is also characterised by high integrated rotation measure, i.e. -800 rad m^{-2}, which can be explained assuming that a magnetised high density medium is present around the radio emission (Taylor et al. 1992). The polarisation properties and rotation measure structure on the arcsecond scale were studied in detail by Owen & Ge (1994). Their images also revealed that the bending region, well visible in Zhao et al. (1993) is not a jet, in that it turns out to be a diffuse and "blobby" emission when observed at higher resolution. In the optical band 3C317 shows several emission line filaments, cospatial with the radio emission (Burns 1990) and its optical spectrum is typical of FRI radio galaxies, i.e. low ionisation and dominant stellar continuum (Tadhunter et al. 1993).

In order to get a clearer picture on the nature of this source we collected all the total flux density data available in the literature and plotted them in Fig. 10 (filled triangles), together with the parsec-scale data we derived in this paper and the values for the arcsecond scale core published in Zhao et al. (1993) and Morganti et al. (1993). Most of the total flux density data were taken from the Kühr Catalogue of Radio Sources (1979). The values at 10, 12.6, 14.7 and 16.7 MHz were taken from Braude et al. (1979). From a few MHz up to ~ 8.4 GHz the total flux density of the source is clearly dominated by the presence of the steep spectrum radio halo ($\alpha_{0.1\,GHz}^{8.4\,GHz} \sim 1.6 \pm 0.1$, Zhao et al. 1993).

Given the arcsecond morphology of 3C317, we chose to observe this source with the EVN+MERLIN at 1.66 GHz and 4.99 GHz, so as to get good sensitivity and u-v coverage at short spacings and ensure the detection of low brightess extended emission on the sub-arcsecond scale, if present. The images we obtained are shown in Figs. 6 to 9 and the details on the images are given in Table 3. Fig. 9 was obtained with the same u-v coverage as Fig. 8, but higher weight was given to the long baselines, in order to better show the structure of the dominant component in Fig. 8.

MERLIN-only images of 3C317 at 1.66 GHZ and 4.99 GHz are shown in Figs. 6 and 7 respectively. The source is barely resolved at both frequencies and resolutions, with an extension in p.a. $\sim -60°$ at 1.66 GHz, and p.a. $\sim 170°$ at 4.99 GHz. The extension in different position angles at different frequencies

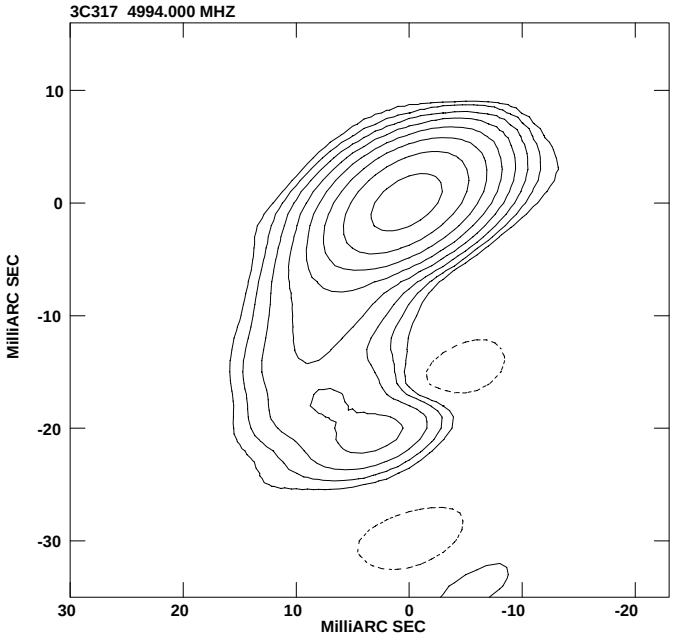

Fig. 8. Full resolution 4.99 GHz EVN+MERLIN image of 3C317. Peak is 216 mJy/beam. Contours: 1.2 mJy/beam × (-1, 1, 2, 4, 8, 16, 32, 64, 128, 256). Beam FWHM: 8.9 × 4.2 (mas) at -70.8°. For this source 1 mas $\sim$ 1 pc.

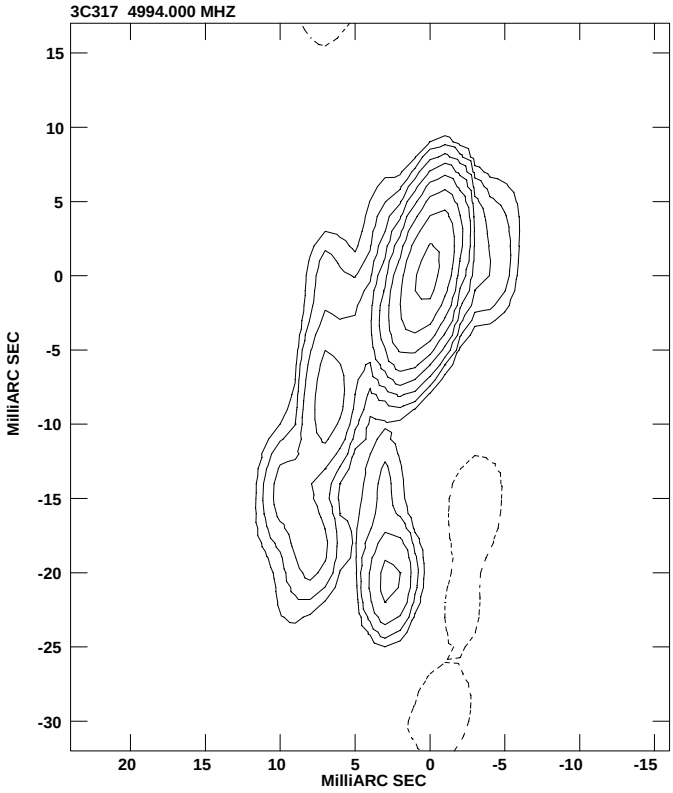

Fig. 9. 4.99 GHz EVN+MERLIN image of 3C317 convolved with FWHM: 5 × 2 (mas) at $0\circ$. Image peak is 165 mJy/beam. Contours are 1.0 mJy/beam × (-1, 1, 2, 4, 8, 16, 32, 64, 128, 256).

and resolutions suggests that the source may have a complex morphology. This is confirmed by our 4.99 GHz full resolution EVN+MERLIN image. At milliarcsecond resolution the source is dominated by a compact component and a jet, bending at ~ 20 mas from the nucleus (i.e. ~ 20 pc). The images shown in Figs. 8 and 9 are very similar to the arcsecond scale ones presented in Zhao et al. (1993), i.e. the jet bends in an anti-clockwise direction on both scales. We present no EVN+MERLIN image at 1.66 GHz since the very noisy EVN data in this observation do not add any information to the MERLIN-only image.

The data presented in this paper are plotted in Fig. 10 together with the PTI data (see Table 3) and the high resolution 8.4 GHz data published in Zhao et al. (1993). Our VLBI data give a spectral index $\alpha_{1.66}^{4.99} \sim 0$ for the total VLBI structure, in agreement with the arcsecond core spectrum derived by Zhao et al. (1993).

On the basis of our observations and from inspection of the plot shown in Fig. 10 we estimate that the core turnover frequency is $\sim$ 5 GHz, however the scatter in the VLA literature data (Morganti et al. 1993; Zhao et al. 1993) for the core does not rule out a flat spectrum, i.e. $\alpha \sim 0$, from 1.6 GHz to 8.4 GHz. We conclude therefore that the steep spectrum radio halo "hides" an active nucleus with flat spectrum.

From Fig. 9 a short counter-jet feature is visible on the opposite side of the main parsec-scale jet, which persisted even though we did not include it in the self-calibration process. We cannot rule out the possibility that it is due to a residual calibration error, however this morphology could also be interpreted in terms of Doppler boosting, as for the other sources presented in this paper (see next section).

5. Discussion and conclusions

Two out of the six radio galaxies from the 2-Jy sample presented in this paper, i.e. PKS 0620−52 and PKS 1333−33, are unresolved at the sensitivity and resolution of the present observations, despite their extended large scale morphology. The extension revealed by a gaussian fit on PKS 1333−33 suggests that some structure exists on the parsec scale, which higher sensitivity observations will probably allow to image.

The remaining four sources show an asymmetric morphology, which could be explained assuming Doppler boosting effects in an intrinsically symmetric source, as from radio loud unified models.

In order to derive estimates for the intrinsic plasma speed $\beta = \frac{v}{c}$ and limits to the viewing angle of the radio source with respect to the line of sight θ, we used two quantities derived from the observations:

(a) the brightness ratio between the parsec-scale jet and counterjet defined as R=$\frac{S_J}{S_{CJ}}$;

(b) the 5 GHz arcsecond scale core dominance with respect to the source total power at 408 MHz (see Table 1), measured comparing the 5 GHz core power logP_c for the sources in our sample to the well known observational relation between logP_c (5 GHz) and logP_{tot} (408 MHz) in low power radio galaxies scaled for our choice of H_o (see Giovannini et al. 1994 for details). In the light of Doppler boosting, the difference between the observed 5 GHz core power and

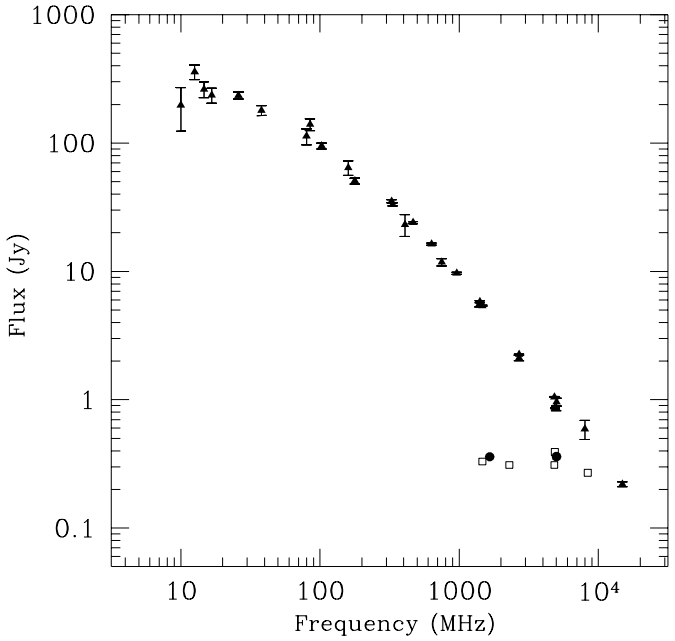

Fig. 10. Spectrum of 3C317 from 10 MHz to 15 GHz. Filled triangles refer to the total flux density; filled circles the VLBI data presented in this paper; open squares are arcsecond core flux density data.

Table 5. Doppler boosting parameters

Source	R	θ_{max}	β_{min}	K	θ_{max}	β_{min}
3C17	$\geq$ 50	49°	0.65	6.31	33°	0.84
PKS 0620−52				2.51	53°	0.60
PKS 0625−35	$\geq$ 12.5	61°	0.47	3.80	43°	0.74
PKS 1318−43	$\geq$ 8	67°	0.40	2.54	53°	0.60
3C317	$\sim$ 4	68°	0.36	6.68	32°	0.85

the core power derived from the correlation, assumed to be the core power for a source oriented at 60° from the line of sight, is entirely due to the different orientation of the radio plasma to the line of sight. As in Giovannini et al. (1994) we define K=$\sqrt{\frac{P_c(\theta)}{P_c(60°)}}$.

In Table 5 we report the limits to the boosting parameters we derived applying these two methods. The ratio R was computed at the distance of the first component reported in Table 4. Since no total flux density measurement is available at 408 MHz for PKS 1318−43, we assumed a value of 16 Jy, derived from extrapolation of the Molonglo 843 MHz flux density with a spectral index α = 1.

Even though the core dominance leads to more stringent limits for β and θ, the values we derived with these two methods are in reasonable agreement with each other, except for 3C317, which we will discuss in further detail below.

3C17 shows the highest degree of asymmetry among our sources, consistent with the fact that it is a broad line radio galaxy, hence expected to be oriented at small to moderate angles to the line of sight.

For PKS 0620−52 the core dominance suggests that the plasma speed in this source can be mildly relativistic to relativistic.

PKS 0625−35 and PKS 1318−43 are both one-sided on the parsec-scale, but their degree of asymmetry is less severe than for 3C17 and leads to upper limits to the viewing angle fully consistent with the expectations from unification. In particular, for PKS 0625−35 the upper limit derived for θ_{max} with both methods is in very good agreement with the independent estimate done by Trussoni et al. (1999). For this source, the upper limit found, coupled with the indication of a hard X–ray unobscured nuclear component, argues in favour of the fact that nuclear obscuration from a torus is probably not relevant in this object.

Interestingly enough, for PKS1333−33 the core power at 5 GHz derived on the basis of the logP$_c$ - logP$_{tot}$ correlation is in perfect agreement with the measured value (see Table 1), thus suggesting that the source is viewed at an angle $\theta \sim 60°$.

The case of 3C317 is more complex. Even though we cannot rule out the possibility that 3C317 is an edge-on radio galaxy with intrinsic bends on the parsec scale amplified by a small viewing angle (see Table 5), an alternative explanation for the properties of 3C317 should also be taken into account. We suggest that the observed bent morphology is the result of the interaction between the relativistic plasma and a very dense external medium. Under this second hypothesis, the parsec-scale jets are disrupted in the sub-arcsecond region, as consequence of gas accretion in the optical counterpart UGC 9799 from the cluster cooling flow, thus preventing the source from evolving into a classical FRI radio galaxy. The MERLIN-only images in Fig. 6 and 7 at 1.66 GHz and at 4.99 GHz respectively show no hint of jets or extended emission at the resolution of the order of 50 mas ($\sim$ 50 pc) at 5 GHz or 150 mas at 1.7 GHz, and this suggests that jet disruption may take place at most at such distance from the core. Zhao et al. (1993) gave estimated the sonic radius r_s for 3C317, i.e. the region where radio jets may become unstable and disrupt as a consequence of the cooling flow at the centre of the galaxy, and gave a value $r_s \leq$0.4 kpc. Our parsec-scale images of 3C317 first of all confirm that the radio plasma is indeed collimated at least out to a distance of $\sim$ 20 pc from the core, moreover they place a new upper limit to the sonic radius $r_s \sim$ 50 pc.

As shown in the previous section, comparison between the nuclear spectrum and the large scale spectrum of 3C317 suggests that a very active nucleus is embedded in a steep spectrum radio halo. If we make the simplified assumption that the parsec-scale emission in the source is in equipartition and if we make the standard equipartition assumptions, i.e. cylindrical geometry, filling factor ϕ = 1, ratio of protons to electrons energy k=1, and integrate in the range of frequencies 10^7–10^{11} Hz, we obtain an estimate for the average parsec-scale magnetic field of the VLBI image B$_{eq}$ $\sim$ 3.5 $\times$ 10^{-3} G. From the core spectrum reported in Fig. 10 we estimated a break frequency $\nu_\star \geq$ 15 GHz, and with the derived value for B$_{eq}$ we obtain a radiative age $t_{syn} \leq$ 2000 yrs. These numbers confirm that the

nuclear region in 3C317 is active, furthermore they suggest that the radiating electrons are very young.

To summarise, the six radio galaxies presented in this paper exhibit parsec-scale properties in agreement with the unified models for radio loud galaxies, i.e. they are characterised by at least mildly relativistic speeds and are viewed at intermediate to large angles to the line of sight.

For 3C17 and PKS 0625−35 our results are in very good agreement with independent estimates derived on the basis of their optical and X-ray properties respectively.

Our detailed study on 3C317 shows that the source is characterised by parsec-scale collimated jets, which disrupt on the sub-kiloparsec region, possibly as consequence of the cooling flow at the centre of the galaxy. Our spectral analysis of the source core region suggests that the source is very young.

Acknowledgements. We thank dr. Daniele Dallacasa for many insightful discussions and critical reading of the manuscript. Thanks are due to M. Tugnoli for his invaluable help in running the Mk2 correlator in Bologna. The Australia Telescope Compact Array (/Parkes telescope/Mopra telescope/Long Baseline array) is part of the Australia Telescope which is funded by the Commonwealth of Australia for operation as a National Facility managed by CSIRO.

References

Barthel P., 1989, ApJ 336, 606
Braude S.Y., Megn A.V., Sokolov K.P., Tkachenko A.P., Sharykin N.K., 1979, Ap&SS 64, 73
Burns J.O., 1990, AJ 99, 14
Capetti A., Celotti A., 1999, MNRAS 304, 434
Chiaberge M., Capetti A., Celotti A., 1999, A&A 349, 77
Chiaberge M., Celotti A., Capetti A., Ghisellini G., 2000, A&A 355, 873
Di Matteo T., Fabian A.C., Rees C.L., Carilli C.L., Ivison R.J., 1999, MNRAS 305, 492
Ekers R.D., Wall J.V., Shaver P.A., et al., 1989, MNRAS 236, 737
Fanaroff B.L., Riley J.M., 1974, MNRAS 167, 31
Feretti L., Giovannini G., Comoretto G., Venturi T., Wehrle A.E., 1993, ApJ 408, 446
Giovannini G., Feretti L., Venturi T., et al., 1994, ApJ 435, 116
Giovannini G., Cotton W.D., Feretti L., Lara L., Venturi T., 1998, ApJ 493, 632
Giovannini G., Taylor G.B., Arbizzani E., et al., 1999, ApJ 519, 108
Ghisellini G., Celotti A., Fossati G., Maraschi L., Comastri A., 1998, MNRAS 301, 451
Jones D.L., Wehrle A.E., 1997, ApJ 484, 186
Killeen N.E.B., Bicknell G.V., Ekers R.D., 1986, ApJ 302, 306
Krichbaum T.P., Alef W., Witzel A., Zensus A.J., Booth R.S., Greve A., Rogers A.E.E., 1998, A&A 329, 873
Kühr H., Nauber U., Pauliny-Toth I.I.K., Witzel A., 1979, Catalogue of Radio Sources. Max Plank Institut für die Radioastronomie, Bonn
Lara L., Cotton W.D., Feretti L., et al., 1997, ApJ 474, 179
Lara L., Feretti L., Giovannini G., Baum S., Cotton W.D., 1999, ApJ 513, 197
Large M.I., Mills B.Y., Little A.G., Crawford D.F., Sutton J.M., 1981, MNRAS 194, 693
Lloyd B.D., Jones P.A., Haynes R.F., 1996, MNRAS 279, 1197
Morganti R., Killeen N., Tadhunter C.N., 1993, MNRAS 263, 1023
Morganti R., Oosterloo T.A., Reynolds J.E., Tadhunter C.N., Migenes V., 1997, MNRAS 284, 541
Morganti R., Oosterloo T.A., Tadhunter C.N., et al., 1999, A&AS 140, 355
Morganti R., Oosterloo T.A., Tadhunter C.N., et al., 2000, MNRAS, in press
Owen F.N., Ge J., 1994, AJ 108, 1523
Padovani P., Morganti R., Siebert J., Vagnetti F., Cimatti A., 1999, MNRAS 304, 829
Pearson T.J., 1991, BAAS 23, 991
Siebert J., Brinkmann W., Morganti R., et al., 1996, MNRAS 279, 1331
Simpson C.J., 1994, Ph.D. Thesis, University of Oxford
Smith R.M., Bicknell G.V., 1986, ApJ 408, 36
Tadhunter C.N., Morganti R., di Serego Alighieri S., Fosbury R.A.E., Danziger I.J., 1993, MNRAS 263, 999
Tadhunter C.N., Dickson R., Morganti R., Villar-Martin M., 1997, In: Clements, Perex-Fournon (eds.) Proceedings of ESO/IAC workshop: Quasar Hosts. p. 311
Tadhunter C.N., Morganti R., Robinson A., et al., 1998, MNRAS 298, 1035
Taylor G.B., Inoue M., Tabara H., 1992, A&A 264, 421
Taylor G.B., 1996, ApJ 470, 394
Trussoni E., Vagnetti F., Massaglia S., et al., 1999, A&A 348, 437
Urry C.M., Padovani P., 1995, PASP 107, 803
Venturi T., Giovannini G., Feretti L., Comoretto G., Wehrle A.E., 1993, ApJ 408, 81
Venturi T., Castaldini C., Cotton W.D., et al., 1995, ApJ 454, 735
Venturi T., Giovannini G., Feretti L., Cotton W.D., Lara L., 2000, Mem. Soc. Astron. Ital. in press
Wall J.V., Peacock J.A, 1985, MNRAS 216, 173
Wright A., Outrupcek R., 1990, Parkes Catalogue. Australia Telescope National Facility
Zhao J.H., Sumi D.M., Burns J.O., Nebojsa D., 1993, ApJ 416, 51